

# Hydrogenlike molecules composed of $D_1D_1$ , $D_1D_2^*$ and $D_2^*D_2^*$

Hu-Hua He, Mao-Jun Yan, Chun-Sheng An, and Cheng-Rong Deng\*

*School of Physical Science and Technology, Southwest University, Chongqing 400715, China*

We systematically explore the S-wave  $D_1D_1$ ,  $D_1D_2^*$  and  $D_2^*D_2^*$  states with various isospin-spin-orbit ( $ISL$ ) configurations in the quark model. We propose nine stable dimeson states with the  $ISL$  configurations,  $ISL = 001, 010, 012, 100, 102, 110, 112, 120$ , and  $122$ , against dissociation into their constituent mesons. Those bound states are hydrogenlike molecular states, where the two subclusters are moderately overlapped and the QCD covalent bond is formed due to the delocalization of light quarks. The QCD covalent bond serves as the primary binding mechanism in the bound states with  $I = 1$ . However, the exchange of  $\pi$  and  $\sigma$ -meson plays a pivotal role in the bound states with  $I = 0$ . The coupled-channel effect is essential in the formation of the bound states with  $ISL = 001, 010, 012, 100$ , and  $102$ .

## I. INTRODUCTION

The history of studying multi-quark states can be traced back to the birth of the quark model in 1964 [1]. Exploring the natures of multi-quark hadrons has been a critically important topic in hadronic physics since Jaffe predicted the H-particle in 1977 [2]. These exotic states may provide a wealth of low-energy strong interaction information that ordinary hadrons do not [3, 4], offering valuable insights into the fundamental nature of these interactions.

In 2003, the Belle Collaboration made a groundbreaking observation of the first narrow hidden charm state very close to the  $D\bar{D}^*$  threshold [5], initially named  $X(3872)$  and now designated as  $\chi_{c1}(3872)$  [6]. This discovery marked a significant milestone in the study of heavy quarkonium states, opening a gate for research into the nature of such kind of exotic states. In the following 20 years, a large amount of hidden charm and hidden bottom hadrons, denoted as  $XYZ$ ,  $P_c$ , and  $P_{cs}$  states, have been continuously observed in experiments [7, 8].

In 2021, the LHCb Collaboration reported the first observation of the doubly charmed tetraquark state  $T_{cc}(3875)^+$  in the  $D^0D^0\pi^+$  invariant mass spectrum [9, 10]. The deuteron-like molecular configuration  $DD^*$  is manifest from its characteristic size [9, 10]. Similar to the hidden charm family, it is anticipated that there exists a diverse array of doubly charmed molecular tetraquarks in hadron spectroscopy. Along these lines, the theorists proposed various types of  $T_{cc}(3875)^+$ -like molecular states, including  $T'_{cc}$  [11],  $T_{bb}^-$  [12–14],  $T_{ccs}^+$  [12, 15–18],  $T_{bc}^0$  [12, 19–22],  $T_{bcs}^0$  [12, 19, 23],  $D_1D_1$  [24, 25],  $D_1D_2^*$  [24] and  $D_2^*D_2^*$  [24]. The LHCb experiment as well as other experiments will provide more chances of observing the hadronic molecules.

One notable and crucial characteristic of the exotic states mentioned above is that they are all positioned very near the thresholds of the hadron pairs to which they can couple. Although the internal structure of

these states remains uncertain and, in some cases, controversial, the prevailing interpretation is that they are hadronic molecular states, with binding energies ranging from several MeV to several tens of MeV [26–29]. The binding mechanisms of these states are complex and involve a range of interactions, including meson exchange, short-range contact forces, and coupled-channel effects, etc. In molecular physics, the covalent bond, formed through the overlap of atomic orbits and the sharing of electrons between atoms, is essential in determining the structure and properties of molecules. Similarly, is there a concept of a “hadronic covalent bond” in the doubly charmed tetraquark systems that resemble the bonding mechanism in the hydrogen molecule?

In our previous study, we analyzed the underlying dynamics involved in the formation of the loosely bound state  $T_{cc}(3875)^+$  and identified the most promising candidates for its partners, which are composed of two ground-state mesons within the quark model. In this study, we extend our model investigation to S-wave dimeson states composed of two excited charmed mesons,  $D_1D_1$ ,  $D_1D_2^*$ , and  $D_2^*D_2^*$ , across various isospin-spin-orbit configurations. Our objective is to explore potential bound states to further enrich the doubly heavy tetraquark family. We will calculate their binding energies, analyze their spatial configurations, and investigate the underlying binding mechanisms. Through this work, we aim to provide valuable insights that could assist in the experimental identification of doubly heavy tetraquark states in the future.

After the Introduction, the paper is organized as follows. In Sec. II, we outline the key characteristics of the quark model. In Sec. III, we provide a brief overview of the trial wave functions for mesons and dimeson states. In Sec. IV, we discuss the properties of the dimeson ground states. Finally, in Sec. V, we conclude with a summary.

## II. QUARK MODEL

The strong interactions are primarily described by quantum chromodynamics (QCD) within the framework

\*Contact author: crdeng@swu.edu.cn

of the standard model of particle physics. However, the *ab initio* calculation of hadron spectroscopy and hadron-hadron interactions directly from QCD is quite challenging due to the complex nonperturbative nature of the theory. This situation has led theoretical physicists to develop various nonperturbative methods to elucidate the dynamics of strong interactions. Among these methods, the quark models have been widely used for decades, offering several advantages, including reduced computational complexity, a clear physical picture, and strong predictive capabilities.

The constituent quark models have been established based on the assumption that hadrons are colorless singlet, non-relativistic bound states of constituent quarks, characterized by phenomenological effective masses and a variety of effective interactions. The origin of the constituent quark mass can be traced back to the spontaneous breaking of  $SU(3)_L \otimes SU(3)_R$  chiral symmetry. As a result, the constituent quarks should interact through the exchange of Goldstone bosons [30]. The chiral symmetry is spontaneously broken in the light quark sector ( $u$ ,  $d$ , and  $s$ ) while being explicitly broken in the heavy quark sector ( $c$  and  $b$ ). Consequently, the Goldstone bosons ( $\pi$ ,  $K$ , and  $\eta$ ) exchange interactions occur only within the light quark sector. Additionally, the scalar meson  $\sigma$  exchange interaction is also involved in the model. The central parts of the interactions can be resummed as follows [31],

$$\begin{aligned}
V_{ij}^{\text{obe}} &= V_{ij}^{\pi} \sum_{k=1}^3 \mathbf{F}_i^k \mathbf{F}_j^k + V_{ij}^K \sum_{k=4}^7 \mathbf{F}_i^k \mathbf{F}_j^k \\
&\quad + V_{ij}^{\eta} (\mathbf{F}_i^8 \mathbf{F}_j^8 \cos \theta_P - \sin \theta_P), \\
V_{ij}^{\chi} &= \frac{g_{ch}^2}{4\pi} \frac{m_{\chi}^3}{12m_i m_j} \frac{\Lambda_{\chi}^2}{\Lambda_{\chi}^2 - m_{\chi}^2} \boldsymbol{\sigma}_i \cdot \boldsymbol{\sigma}_j \\
&\quad \times \left( Y(m_{\chi} r_{ij}) - \frac{\Lambda_{\chi}^3}{m_{\chi}^3} Y(\Lambda_{\chi} r_{ij}) \right), \quad Y(x) = \frac{e^{-x}}{x} \\
V_{ij}^{\sigma} &= -\frac{g_{ch}^2}{4\pi} \frac{\Lambda_{\sigma}^2 m_{\sigma}}{\Lambda_{\sigma}^2 - m_{\sigma}^2} \left( Y(m_{\sigma} r_{ij}) - \frac{\Lambda_{\sigma}}{m_{\sigma}} Y(\Lambda_{\sigma} r_{ij}) \right).
\end{aligned} \tag{1}$$

Besides the chiral symmetry breaking, it is expected that the dynamics of the model are governed by QCD. The perturbative effect is primarily represented by the well-known one-gluon exchange (OGE) interaction. From the nonrelativistic reduction of the OGE diagram in QCD for point-like quarks, we obtain the following expression,

$$V_{ij}^{\text{oge}} = \frac{\alpha_s}{4} \boldsymbol{\lambda}_i^c \cdot \boldsymbol{\lambda}_j^c \left( \frac{1}{r_{ij}} - \frac{2\pi\delta(\mathbf{r}_{ij})\boldsymbol{\sigma}_i \cdot \boldsymbol{\sigma}_j}{3m_i m_j} \right), \tag{2}$$

where  $\boldsymbol{\lambda}_i^c$  and  $\boldsymbol{\sigma}_i$  represent the color  $SU(3)$  Gell-Mann matrices and the spin  $SU(2)$  Pauli matrices, respectively. Here,  $r_{ij}$  denotes the distance between quarks  $i$  and  $j$ , and  $m_i$  is the mass of the  $i$ -th quark.

Finally, any model that aims to mimic QCD must incorporate the nonperturbative effect of color confine-

ment. We adopt a phenomenological color screening confinement potential to address this requirement,

$$\begin{aligned}
V_{ij}^{\text{con}} &= -a_c \boldsymbol{\lambda}_i^c \cdot \boldsymbol{\lambda}_j^c f(r_{ij}) \\
f(r_{ij}) &= \begin{cases} r_{ij}^2 & \text{if } i, j \text{ occur in the same meson,} \\ \frac{1 - e^{-\mu_c r_{ij}^2}}{\mu_c} & \text{if } i, j \text{ occur in different mesons.} \end{cases}
\end{aligned}$$

This type of hybrid confinement potential arises from the quark delocalization and color screening model [32, 33], which can effectively describe the nuclear intermediate-range attraction. It also reproduces nucleon-nucleon scattering data and the properties of the deuteron [32, 33]. Recently, this model has successfully described the properties of the  $T_{cc}^+$  state observed by the LHCb Collaboration [12].

### III. WAVE FUNCTIONS

The wave function of a colorless charmed meson with isospin  $I$  and angular momentum  $J$  can be expressed as the direct product of its constituent parts: the color part  $\chi_c$ , the isospin part  $\eta_i$ , the spin part  $\psi_s$ , and the spatial part  $\phi_{lm}^G(\mathbf{r})$ . This can be written mathematically as

$$\Phi_{IJ}^D = \chi_c \otimes \eta_i \otimes \psi_s \otimes \phi_{lm}^G(\mathbf{r}), \tag{3}$$

where  $D$  stands for all possible charmed mesons, encompassing both ground states and excited states.  $\mathbf{r}$  is the relative coordinate between the quarks  $c$  and  $\bar{q}$ , where  $\bar{q}$  represent either  $\bar{u}$  or  $\bar{d}$  in the context of the  $D$  meson.

To obtain a reliable solution to the few-body problem, a high-precision numerical method is essential. The Gaussian Expansion Method (GEM) has proven to be a highly effective tool for solving few-body problems [34, 35]; thus, in this study, we employ the GEM to investigate the doubly heavy tetraquark system. According to the GEM, the relative motion wave function can be written as a superposition of a set of Gaussian functions with specified angular momentum,

$$\phi_{lm}^G(\mathbf{r}) = \sum_{n=1}^{n_{\text{max}}} c_n N_n l r^l e^{-\nu_n r^2} Y_{lm}(\hat{\mathbf{r}}),$$

More details about the GEM can be found in Refs. [34, 35].

The doubly charmed molecular states, denoted as  $T_{cc}$ , can be established by the colorless mesons  $D_1$  (composed of  $c_1 \bar{q}_1$ ) and  $D_2$  (composed of  $c_2 \bar{q}_2$ ), where the indices just denote the specific particles rather than their angular momentum. The wave function of the states with defined isospin  $I$  and total angular momentum  $J$  can be expressed as

$$\Psi_{IJ}^{T_{cc}} = \sum_{\xi} c_{\xi} \mathcal{A}_{12} \left\{ \left[ \Phi_{I_1 J_1}^{D_1} \Phi_{I_2 J_2}^{D_2} \right]_{IJ} \phi_{lm}^G(\boldsymbol{\rho}) \right\}. \tag{4}$$

The term  $\phi_{lm}^G(\boldsymbol{\rho})$  represents the wave function for the relative motion between the two mesons in the center-of-mass frame. The Jaccobi coordinate  $\boldsymbol{\rho}$  can be explicitly expressed as

$$\boldsymbol{\rho} = \frac{m_c \mathbf{r}_{c_1} + m_{\bar{q}} \mathbf{r}_{\bar{q}_1}}{m_c + m_{\bar{q}}} - \frac{m_c \mathbf{r}_{c_2} + m_{\bar{q}} \mathbf{r}_{\bar{q}_2}}{m_c + m_{\bar{q}}}. \quad (5)$$

Similarly, this wave function can be expanded as a superposition of a set of Gaussian functions. In this work, we primarily focus on the ground state of our systems, as it is more likely to form a bound state [26].

The square brackets indicate the Clebsch-Gordan couplings of angular momentum and isospin. The operator  $\mathcal{A}_{12}$  serves as an antisymmetrization operator that acts on the identical quarks  $c_1$  and  $c_2$ , as well as on the identical anti-quarks  $\bar{q}_1$  and  $\bar{q}_2$ .

$$\mathcal{A}_{12} = (1 - P_{c_1 c_2})(1 - P_{\bar{q}_1 \bar{q}_2}), \quad (6)$$

where  $P$  is the permutation operator acting on the identical particles. The summation index  $\xi$  encompasses all possible isospin-spin intermediate configurations  $\{I_1, I_2, J_1, J_2\}$  that can be coupled to yield the total isospin  $I$  and angular momentum  $J$  of the state  $T_{cc}$ . The coefficients  $c_\xi$  can be determined through the dynamics of the model. To satisfy Bose-Einstein statistics, a restriction must be imposed on the quantum numbers  $\{I_1, I_2, J_1, J_2\}$  when the mesons  $D_1$  and  $D_2$  are identical bosons. Their quantum numbers must satisfy the relation  $J_1 + J_2 - J + I_1 + I_2 - I = \text{even}$ .

## IV. NUMERICAL RESULTS AND ANALYSIS

### A. Methodology

The first step in studying tetraquark systems is to incorporate ordinary mesons within the quark model in order to determine the model parameters. By accurately solving the two-body Schrödinger equation, we have reproduced the mass spectrum of ground state ordinary mesons [36].

TABLE I: Meson spectrum, mass unit is in MeV and  $\langle r^2 \rangle^{\frac{1}{2}}$  unit in fm.

State	$D$	$D^*$	$D_1$	$D_2^*$	$D_3^*$	$B$	$B^*$	$B_1$	$B_2^*$
$IJ^P$	$\frac{1}{2}0^-$	$\frac{1}{2}1^-$	$\frac{1}{2}1^+$	$\frac{1}{2}2^+$	$\frac{1}{2}3^-$	$\frac{1}{2}0^-$	$\frac{1}{2}1^-$	$\frac{1}{2}1^+$	$\frac{1}{2}2^+$
Cal.	1867	2002	2361	2368	2677	5259	5301	5666	5668
PDG.	1869	2007	2420	2460	2750	5280	5325	5721	5747
$\langle r^2 \rangle^{\frac{1}{2}}$	0.68	0.82	1.16	1.17	1.45	0.73	0.77	1.13	1.14

Based on the model parameters obtained from fitting the ground-state meson spectrum [36], we present the masses of the nonstrange charmed and bottomed excited mesons in Table I.  $D_0$  is absent because it has a very

large width, which prevents it from being a good building block of hadronic molecules. It is worth noting that the mass difference between the experimental data and the model predictions for the excited states is on the order of several tens of MeV. However, this discrepancy does not significantly impact the binding energy of the dimeson states, due to the specific definition of reduction used in the calculation, see Eq. (8).

Utilizing the quark model, we then investigate the state  $T_{cc}(3875)^+$  observed by the LHCb Collaboration. Our analysis indicates that the model describes the state  $T_{cc}(3875)^+$  as a loosely bound, deuteron-like state within the quark framework, a description that aligns remarkably well with the experimental data [12].

Next, we turn our attention to the investigation of the dimeson states  $T_{cc}$ , composed of two excited charmed states within the quark model. Generally, orbitally excited bound states are more difficult to form due to the repulsive centrifugal potential. Therefore, this study will focus on the ground states  $T_{cc}$  with various isospin-spin-orbit configurations, where two excited charmed mesons are in the relative  $S$ -wave. To obtain the eigenvalues and eigenvectors of the dimeson states  $T_{cc}$ , we solve the four-body Schrödinger equation

$$(H_4 - E_4)\Psi_{IJ}^{T_{cc}} = 0 \quad (7)$$

for the bound-state problem with the Rayleigh-Ritz variational principle.

The binding energy  $\Delta E_4$  of the states  $T_{cc}$  is defined as

$$\Delta E_4 = E_4 - \lim_{\rho \rightarrow \infty} E_4(\rho) \quad (8)$$

This expression is applied to determine whether the states  $T_{cc}$  are stable against the strong interactions. Here,  $E(\infty)$  represents the theoretical threshold corresponding to the energy of two completely separated mesons that can couple to the same quantum numbers as the dimeson states  $T_{cc}$ . This subtraction can procedure significantly reduces the influence of uncertainties in model parameters and meson spectra on the calculated binding energies. If  $\Delta E_4 \geq 0$ , the state  $T_{cc}$  is unbound and can decay into two constituent mesons via strong interactions. However, if  $\Delta E_4 < 0$ , the strong decay into two constituent mesons is forbidden, and the decay can only occur via weak or electromagnetic interactions.

We present the binding energies of the dimeson states with various isospin-spin-orbit configurations in Table II. In the present calculation, we consider only the spin-spin and orbit-orbit couplings, neglecting the spin-orbit coupling. Based on prior experience, the mass splitting caused by the spin-orbit interaction is deemed negligible [37, 38]. A more comprehensive investigation into the effects of spin-orbit coupling is left for future studies.

To provide a clearer and more intuitive representation of the energy spectrum, the binding energies of these dimeson states, relative to their constituent mesons, are displayed in Fig. 1. The thresholds for  $D_1 D_1$ ,  $D_1 D_2^*$ , and  $D_2^* D_2^*$  are indicated by dotted horizontal lines. This

visualization offers a better understanding of the relative binding energies and the positioning of each state in relation to the respective thresholds.

To clarify the binding mechanism of the bound states, we analyze the contributions from various interactions  $\Delta\langle V^\chi \rangle$  and kinetic energy  $\Delta T$  to the binding energy  $\Delta E_4$  using its eigenvector,

$$\begin{aligned} \Delta\langle V^\chi \rangle = & \langle \Psi_{I_1 J_1}^{T_{cc}} | V^\chi | \Psi_{I_1 J_1}^{T_{cc}} \rangle - \langle \Phi_{I_1 J_1}^{D_1} | V^\chi | \Phi_{I_1 J_1}^{D_1} \rangle \\ & - \langle \Phi_{I_2 J_2}^{D_2} | V^\chi | \Phi_{I_2 J_2}^{D_2} \rangle, \end{aligned} \quad (9)$$

where  $\chi$  represents all types of interactions in the quark model. In order to reveal the spatial configuration, we compute the size of the mesons and the distances between two mesons in the dimeson state  $T_{cc}$ . The numerical results from these calculations are presented in Table II.

### B. S-wave $D_1 D_1$ state

It can be observed from Table II that the S-wave  $D_1 D_1$  state with the two isospin-spin-orbit configurations  $ISL = 001$  ( $IJ^P = 01^+$ ) and  $102$  ( $IJ^P = 12^+$ ) is not able to form a bound state because of the absence of attraction within the quark model. In stark contrast, the S-wave  $D_1 D_1$  state, characterized by the configuration  $ISL = 100$ , is predicted to form a bound state with a binding energy of around 5.59 MeV relative to its constituent  $D_1 D_1$  in the quark model. In this bound state, the majority of the attraction arises from the  $\sigma$ -meson exchange, confinement potential and chromomagnetic interaction. Additionally, the kinetic energy,  $\pi$ - and  $\eta$ -meson exchange provide small attractive contributions, less than 1 MeV. However, the coulomb interaction introduces some repulsions, about 3.29 MeV.

Both the one-boson exchange model and chiral perturbation theory have also explored the S-wave  $D_1 D_1$  state with  $IJ^P = 01^+$ ,  $02^+$ , and  $10^+$  at the meson level [24, 25, 27]. Their conclusions contrast with the present work, which finds that the isospin singlet is more likely to form a bound state than the isospin triplet. The  $D_1 D_1$  state with  $IJ^P = 01^+$  can form a shallow bound state with a molecular configuration when the cutoff parameter  $\Lambda$  is small [24, 25, 27]. In Refs. [24, 27], the S-wave  $D_1 D_1$  state with  $IJ^P = 10^+$  and  $12^+$  does not form a bound state. However, in Ref. [25], while the S-wave  $D_1 D_1$  state with  $IJ^P = 10^+$  does not form a bound state, the S-wave  $D_1 D_1$  state with  $IJ^P = 12^+$  can establish a loosely bound state after including recoil corrections.

In general, the relative kinetic energy tends to be repulsive, preventing the constituent particles from forming a bound state in few-body quantum systems [39–43]. The relative kinetic energy, acting as a novel binding mechanism in this bound state, can be understood by examining the spatial configuration of the bound state. The size of the two subclusters,  $D_1 D_1$  pair, is approximately 1.16 fm, and the distance between them is about 1.89 fm. As

a result, the two subclusters slightly overlap. This spatial overlap increases the phase space available for the light quarks  $\bar{q}_1$  and  $\bar{q}_2$ , allowing them to move freely into the opposite subcluster. This contributes to the reduction of the kinetic energy of the bound state, which exemplifies the realization of the uncertainty principle.

The delocalization of the light quarks in the bound state closely resembles that of the electrons in the hydrogen molecule, where the two hydrogen atoms are bound through the valence bond formed by the delocalization of the two electrons. In this sense, the bound state  $D_1 D_1$  with  $ISL = 100$  is a hydrogenlike molecule state, where the QCD valence bond formed through the delocalization of the light quarks although it is weaker than the  $\sigma$ -meson exchange, confinement potential and chromomagnetic interaction. The formation of the QCD valence bond arises from the exchange of light quarks, which ensures adherence to the Pauli exclusion principle. The concept of the QCD valence bond was proposed by analogy with the hydrogen molecule in 2013 [44]. More recently, the QCD valence bond, along with other types of QCD bonds in multiquark hadrons, has been extensively discussed in the literature [45, 46].

### C. S-wave $D_1 D_2^*$ state

The S-wave  $D_1 D_2^*$  state possesses six isospin-spin-orbit configurations, as illustrated in Table II, due to the absence of constraints imposed by Bose-Einstein statistics. The S-wave  $D_1 D_2^*$  state with  $ISL = 010$  ( $IJ^P = 01^+$ ),  $011$  ( $IJ^P = 00^+$ ,  $01^+$ ,  $02^+$ ),  $012$  ( $IJ^P = 01^+$ ,  $02^+$ ,  $03^+$ ), and  $111$  ( $IJ^P = 10^+$ ,  $11^+$ ,  $12^+$ ) cannot form any bound states because of the lack of sufficient binding mechanisms within the quark model.

The S-wave  $D_1 D_2^*$  state with  $ISL = 110$  ( $IJ^P = 11^+$ ) can form a deeply bound state with an approximate binding energy of 19.40 MeV within the quark model. In this bound state, the majority of the attraction, about 11.8 MeV, comes from the kinetic energy, as shown in Table II. Additionally, the confinement potential also provide a strong attraction, about 8.70 MeV. The contributions from the meson exchanges ( $\sigma$ -,  $\pi$ -, and  $\eta$ -meson) and chromomagnetic interaction provide only small attractive effects. However, the Coulomb interaction leads to a strongly repulsive effect of about 8.21 MeV.

The distance between the two subclusters,  $D_1$  and  $D_2^*$ , is 1.39 fm, indicating a strong overlap between the subclusters. By comparison, we observe that even if all other interactions are switched off, leaving only the kinetic energy and Coulomb interaction, the system is still able to form a bound state. In this sense, a strong QCD valence bond appears, making this bound state resemble a hydrogen-like molecular state.

The S-wave  $D_1 D_2^*$  state with  $ISL = 112$  ( $IJ^P = 11^+$ ,  $12^+$ ,  $13^+$ ) can generate a shallow bound state, exhibiting an approximate binding energy of 3.58 MeV, in the quark model. The kinetic energy still plays a decisive

TABLE II: Binding energy  $\Delta E_4$  of the dimeson states relative to their constituents and the contribution from various interactions and kinetic energy, unit in MeV.  $\Delta V^\sigma$ ,  $\Delta V^\pi$ ,  $\Delta V^\eta$ ,  $\Delta V^{\text{con}}$ ,  $\Delta V^{\text{cm}}$ ,  $\Delta V^{\text{coul}}$ , and  $\Delta T$  represent  $\sigma$ -,  $\pi$ -, and  $\eta$ -meson term, confinement term, chromomagnetic term, Coulomb term, and kinetic energy, respectively.  $I$ ,  $S$  and  $L$  represent total isospin, spin, orbital angular momentum, respectively.  $\langle r^2 \rangle^{\frac{1}{2}}$  is the size of mesons and  $\langle \rho^2 \rangle^{\frac{1}{2}}$  is the distance between two mesons, unit in fm.

Constituent	$I, S \oplus L$	$\Delta E_4$	$\langle r^2 \rangle^{\frac{1}{2}}$	$\langle \rho^2 \rangle^{\frac{1}{2}}$	$\Delta V^\sigma$	$\Delta V^\pi$	$\Delta V^\eta$	$\Delta V^{\text{con}}$	$\Delta V^{\text{cm}}$	$\Delta V^{\text{coul}}$	$\Delta T$
$D_1 D_1$	$0, 0 \oplus 1$	Unbound									
	$1, 0 \oplus 0$	-5.59	1.15	1.89	-2.78	-0.34	-0.11	-2.77	-2.01	3.29	-0.86
	$1, 0 \oplus 2$	Unbound									
$D_1 D_2^*$	$0, 1 \oplus 0$	Unbound									
	$0, 1 \oplus 1$	Unbound									
	$0, 1 \oplus 2$	Unbound									
	$1, 1 \oplus 0$	-19.40	1.13	1.39	-3.83	-1.29	-0.26	-8.70	-1.72	8.21	-11.80
	$1, 1 \oplus 1$	Unbound									
$D_2^* D_2^*$	$1, 1 \oplus 2$	-3.58	1.15	1.99	-2.96	-0.96	-0.19	-1.11	-1.38	9.33	-6.31
	$0, 0 \oplus 1$	-1.11	1.17	2.78	-1.76	-1.81	-0.01	-1.54	-2.09	0.30	5.81
	$0, 1 \oplus 0$	Unbound									
	$0, 1 \oplus 2$	Unbound									
	$0, 2 \oplus 1$	Unbound									
	$1, 0 \oplus 0$	Unbound									
	$1, 0 \oplus 2$	Unbound									
	$1, 2 \oplus 0$	-19.55	1.14	1.40	-3.78	-1.27	-0.26	-8.85	-1.86	8.21	-11.70
	$1, 1 \oplus 1$	Unbound									
$1, 2 \oplus 2$	-3.69	1.16	1.96	-2.96	-0.96	-0.18	-1.20	-1.50	9.44	-6.33	

TABLE III: Channel coupled effects for the bound states with the same  $ISL$  and sole bound channel, see the caption for Table II.

Constituent	$I, S \oplus L$	Ratio	$\Delta E_4$	$\langle r^2 \rangle^{\frac{1}{2}}$	$\langle \rho^2 \rangle^{\frac{1}{2}}$	$\Delta V^\sigma$	$\Delta V^\pi$	$\Delta V^\eta$	$\Delta V^{\text{con}}$	$\Delta V^{\text{cm}}$	$\Delta V^{\text{coul}}$	$\Delta T$
$D_1 D_1$	$0, 0 \oplus 1$	55%	-3.03	1.15	1.73	-2.67	-5.18	0.08	0.03	2.84	5.69	-3.83
$D_2^* D_2^*$		45%										
$D_1 D_2^*$	$0, 1 \oplus 0$	56%	-18.61	1.13	1.34	-4.05	-12.52	0.86	-8.46	8.74	9.56	-12.72
$D_2^* D_2^*$		44%										
$D_1 D_2^*$	$0, 1 \oplus 2$	71%	-2.42	1.15	2.02	-3.03	-8.84	0.58	-0.77	6.32	9.97	-6.65
$D_2^* D_2^*$		29%										
$D_1 D_1$	$1, 0 \oplus 0$	85%	-16.41	1.13	1.41	-3.80	-1.26	-0.26	-6.19	0.82	9.19	-14.90
$D_2^* D_2^*$		15%										
$D_1 D_1$	$1, 0 \oplus 2$	95%	-1.79	1.15	2.25	-2.46	-0.72	-0.15	-0.04	-0.30	7.55	-5.67
$D_2^* D_2^*$		5%										
$D_1 D_2^*$	$1, 1 \oplus 0$	Sole	-19.40	1.13	1.39	-3.83	-1.29	-0.26	-8.70	-1.72	8.21	-11.80
$D_1 D_2^*$	$1, 1 \oplus 2$	Sole	-3.58	1.15	1.99	-2.96	-0.96	-0.19	-1.11	-1.38	9.33	-6.31
$D_2^* D_2^*$	$1, 2 \oplus 0$	Sole	-19.55	1.14	1.40	-3.78	-1.27	-0.26	-8.85	-1.86	8.21	-11.70
$D_2^* D_2^*$	$1, 2 \oplus 2$	Sole	-3.69	1.16	1.96	-2.96	-0.96	-0.18	-1.20	-1.50	9.44	-6.33

role in the formation of the bound state, as shown in Table II. Additionally, the  $\sigma$ -meson exchange provides a strong attraction, contributing approximately 2.96 MeV. The meson exchanges ( $\pi$  and  $\eta$ -meson), chromomagnetic

interaction, and confinement potential each contribute only small attractive effects. In contrast, the Coulomb interaction results in a strongly repulsive effect, approximately 9.33 MeV. The distance between the two subclus-

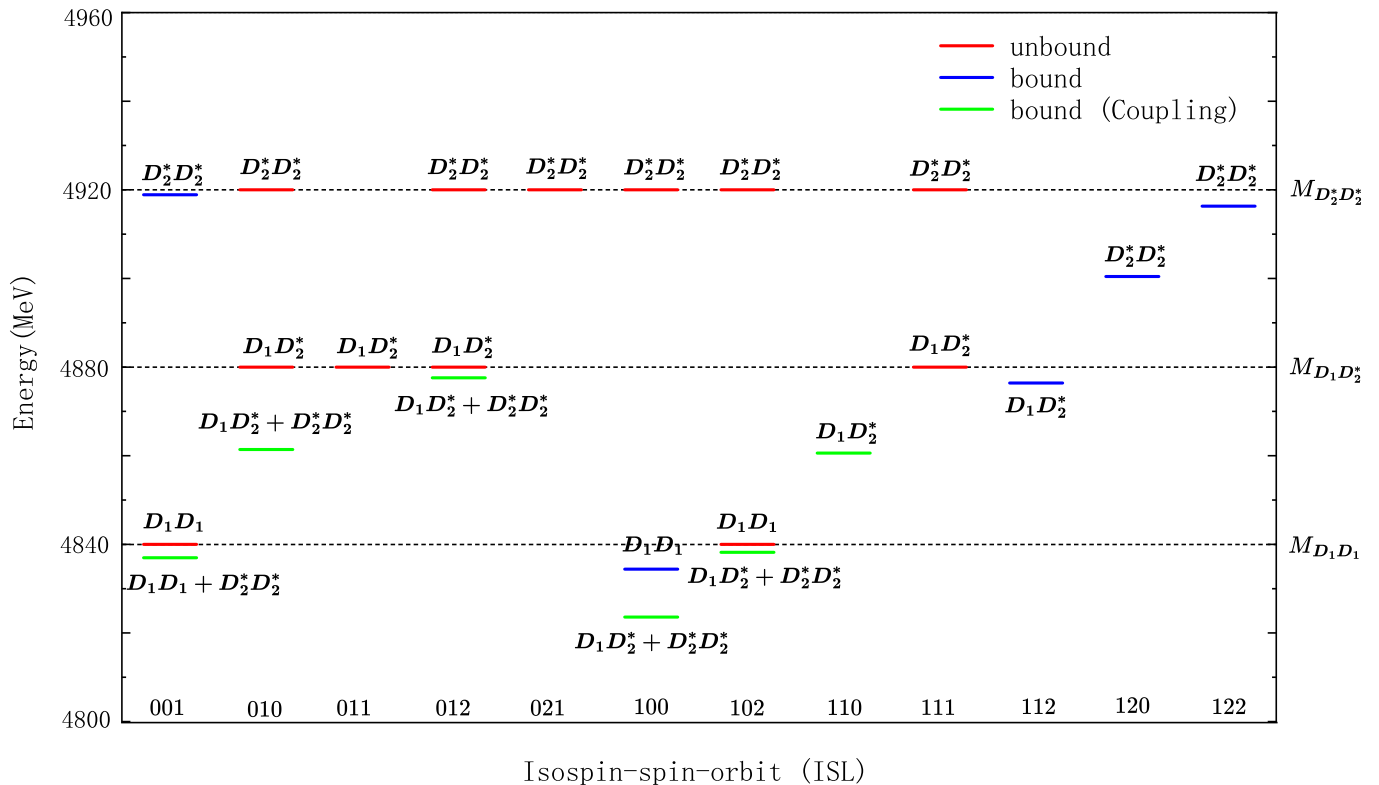


FIG. 1: The energy spectrum of the dimeson states  $D_1D_1$ ,  $D_1D_2^*$ , and  $D_2^*D_2^*$  with various isospin-spin-orbit configurations. The thresholds  $M_{D_1D_1}$ ,  $M_{D_1D_2^*}$ , and  $M_{D_2^*D_2^*}$  are marked by three dotted horizontal lines. The red and blue line represents the single channel while the green line stands for the result for the mixing of two channels with the same  $ISL$ .

ters,  $D_1$  and  $D_2^*$ , is 1.99 fm, indicating a slightly overlap between the subclusters. Consequently, this bound state can also be described as a hydrogen-like molecular state.

In the chiral perturbation theory, all isoscalar S-wave  $D_1D_2^*$  states can form bound states, whereas for all isovector states, the potential arising from  $\rho$  and  $\omega$  exchange is repulsive, thereby preventing the formation of molecular states [27]. In the one-boson-exchange model, the S-wave  $D_1D_2^*$  state with  $IJ^P = 01^+$  and  $02^+$  is easy to form a bound state while the state with  $13^+$  can generate a bound state under the condition of large cutoff parameter [24]. These conclusions are in stark contrast to the results obtained in the present study. The primary reason for these differences lies in the obviously distinct binding mechanisms underlying the formation of the bound states.

#### D. S-wave $D_2^*D_2^*$ state

The S-wave  $D_2^*D_2^*$  state has nine isospin-spin-orbit configurations, as shown in Table II, because of the constraints imposed by Bose-Einstein statistics. Among these, only three configurations  $ISL = 001$  ( $IJ^P = 01^+$ ),  $120$  ( $IJ^P = 12^+$ ), and  $122$  ( $IJ^P = 10^+, 12^+, 14^+$ ) are ca-

pable of forming a bound state in the quark model. The remaining configurations are unbound due to the absence of sufficient binding mechanisms.

The S-wave  $D_2^*D_2^*$  state with  $ISL = 001$  is a shallow bound state, possessing a binding energy of approximately 1.11 MeV. This state is notably distinct from the other bound states discussed earlier, as the primary factor inhibiting the formation of the  $D_2^*D_2^*$  pair into a bound state is the kinetic energy. The distance between the two subclusters is approximately 2.78 fm, which is greater than the size of each subcluster, suggesting that this bound state resembles a deuteron-like molecule. In this bound state, the interaction between the two subclusters arises from the exchange of  $\pi$ - and  $\sigma$ -mesons, along with the confinement potential and chromomagnetic interaction. In the chiral perturbation theory and one boson exchange model, the S-wave  $D_2^*D_2^*$  state with  $IJ^P = 01^+$  and  $03^+$  can generate bound molecular states [24, 27].

The S-wave  $D_2^*D_2^*$  state with  $ISL = 120$  can lead to the formation of a deep bound state within the quark model, whereas the state with  $ISL = 122$  corresponds to a shallow bound state. Upon comparison, we observe that their properties, including binding energy, binding mechanisms, and spatial configurations, are strik-

ingly similar to those of the S-wave  $D_1D_2^*$  state with  $ISL = 110$  and  $ISL = 112$ , respectively, as shown in Table II. As a result, the S-wave  $D_2^*D_2^*D$  states with  $ISL = 120$  and  $122$  can be described as hydrogen-like molecular states in the quark model. In the one-boson exchange model, the S-wave  $D_2^*D_2^*D$  state with  $IJ^P = 14^+$  can form a bound molecular state [24]. However, the states with  $IJ^P = 10^+$  and  $12^+$  exhibit weak attraction or repulsion, depending on the variation of the cutoff parameter within the range of 0.80 to 2.50 GeV [24].

### E. Coupled channel effects

From a quantum mechanical perspective, the dimeson states should be the linear combinations of all possible isospin-spin-orbit configurations allowed by their quantum numbers. The mixing of these configurations may lead to a lowering of the energy of the dimeson states. In this context, we carry out coupling calculations involving the states that share the same isospin-spin-orbit configurations in Table II. The numerical results of the coupling calculations for the bound states are presented in Table III and Fig. 1.

The coupled binding energy for the S-wave  $D_1D_1$  and  $D_2^*D_2^*$  states with  $ISL = 001$  ( $IJ^P = 01^+$ ) is approximately 3.03 MeV below the  $D_1D_1$  threshold. In the bound state, the contribution of  $D_1D_1$  is slightly larger than that of  $D_2^*D_2^*$ . Similarly, the S-wave  $D_1D_2^*$  and  $D_2^*D_2^*$  states with  $ISL = 010$  ( $IJ^P = 01^+$ ) and  $012$  ( $IJ^P = 01^+, 03^+$ ) can also generate bound states relative to the  $D_1D_2^*$  threshold when the coupled-channel effect is taken into account. Their coupled binding energies are 18.61 MeV and 2.42 MeV, respectively, with the dominant component being  $D_1D_2^*$ . The coupled-channel effect is essential in the formation of those bound states, significantly influencing their existence.

The coupled binding energies for the S-wave  $D_1D_1$  and  $D_2^*D_2^*$  states with  $ISL = 100$  ( $IJ^P = 10^+$ ) and  $102$  ( $IJ^P = 20^+$ ) are approximately 16.41 MeV and 1.79 MeV lower than the  $D_1D_1$  threshold, respectively. In both bound states, the dominant component is  $D_1D_1$ , as shown in Table III. The coupled-channel effect significantly lowers the energy of the bound state  $D_1D_1$  with  $ISL = 100$ , even though it could form a bound state independently. The formation of the shallow bound state with  $ISL = 102$  is entirely dependent on the coupled-channel effect.

The exchange of  $\pi$  and  $\sigma$ -meson plays a pivotal role in the bound states with  $I = 0$ , as they account for the majority of the attractive forces, as demonstrated in Table III. Additionally, the kinetic energy contributes sig-

nificantly to the overall attraction. In contrast, the situation for the bound states with  $I = 1$  differs markedly. The kinetic energy serves as the primary binding mechanism in the bound states with  $I = 1$ , as it provides the majority of the attraction. In comparison, the exchange of  $\pi$  and  $\sigma$ -meson is relatively secondary even trivial. In this context, it is challenging to form bound states with isospin  $I = 1$  at the meson level, as the quark degrees of freedom are effectively frozen in both the one-boson exchange model and chiral perturbation theory. In the bound states in Table III, the two subclusters overlap to some extent, making these bound states resemble hydrogen-like molecules within the quark model.

## V. SUMMARY

In this study, we systematically investigate the properties of the S-wave states  $D_1D_1$ ,  $D_1D_2^*$  and  $D_2^*D_2^*$  with various isospin-spin-orbit configurations in the quark model utilizing the Gaussian expansion method. By precisely solving the fourbody Schrödinger equations for the bound state question, we propose nine possible bound states with the isospin-spin-orbit configurations,  $ISL = 001, 010, 012, 100, 102, 110, 112, 120,$  and  $122$ , against dissociation into their constituent mesons.

Those bound states are hydrogenlike molecular states, where the QCD covalent bond is formed due to the delocalization of light quarks. The QCD covalent bond serves as the primary binding mechanism in the bound states with  $I = 1$ . Those bound states with  $I = 1$  cannot form in both the one-boson exchange model and chiral perturbation theory because the quark degrees of freedom are effectively frozen. In contrast, the exchange of  $\pi$  and  $\sigma$ -meson plays a pivotal role in the bound states with  $I = 0$ . The coupled-channel effect is essential in the formation of the bound states with  $ISL = 001, 010, 012, 100,$  and  $102$ , significantly influencing their existence.

The information regarding the bound states presented in this work is expected to provide valuable assistance and guidance for future experimental efforts aimed at exploring the existence of exotic hadronic states.

### Acknowledgments

This research is supported by the National Natural Science Foundation of China under Grants No. 12305096, the Fundamental Research Funds for the Central Universities under Grant No. SWU-XDJH202304 and No. SWU-KQ25016.

[1] M. Gell-Mann, Phys. Lett. **8**, 214 (1964).  
[2] R.L. Jaffe, Phys. Rev. Lett. **38**, 195 (1977).

[3] R.L. Jaffe, Phys. Rept. **409**, 1 (2005).  
[4] S.L. Olsen, T. Skwarnicki and D. Zieminska, Rev. Mod.

- Phys. **90**, 015003 (2018).
- [5] S.K. Choi *et al.* [Belle], Phys. Rev. Lett. **91**, 262001 (2003).
- [6] T. Gershon [LHCb], arXiv:2206.15233 [hep-ex].
- [7] H.X. Chen, W. Chen, X. Liu and S.L. Zhu, Phys. Rept. **639**, 1 (2016).
- [8] N. Brambilla, S. Eidelman, C. Hanhart, A. Nefediev, C.P. Shen, C.E. Thomas, A. Vairo and C.Z. Yuan, Phys. Rept. **873**, 1 (2020).
- [9] R. Aaij *et al.* [LHCb], Nature Phys. **18**, 751 (2022).
- [10] R. Aaij *et al.* [LHCb], Nature Commun. **13**, 3351 (2022).
- [11] R. Chen, Q. Huang, X. Liu and S.L. Zhu, Phys. Rev. D. **104**, 114042 (2021).
- [12] C.R. Deng and S.L. Zhu, Phys. Rev. D. **105**, 054015 (2022).
- [13] M. Albaladejo, Phys. Lett. B. **829**, 137052 (2022).
- [14] T. Aoki, S. Aoki and T. Inoue, Phys. Rev. D. **108**, 054502 (2023).
- [15] M. Karliner and J.L. Rosner, Phys. Rev. D. **105**, 034020 (2022).
- [16] L.R. Dai, R. Molina and E. Oset, Phys. Rev. D **105**, 016029 (2022), [erratum: Phys. Rev. D. **106**, 099902 (2022)].
- [17] Y. Li, Y.B. He, X.H. Liu, B. Chen and H.W. Ke, Eur. Phys. J. C. **83**, 258 (2023).
- [18] M. Tanaka, Y. Yamaguchi and M. Harada, Phys. Rev. D. **110**, 016024 (2024).
- [19] N. Mathur and M. Padmanath, PoS. **LATTICE2021**, 443 (2022).
- [20] C. Alexandrou, J. Finkenrath, T. Leontiou, S. Meinel, M. Pflaumer and M. Wagner, Phys. Rev. Lett. **132**, 151902 (2024).
- [21] M. Padmanath, A. Radhakrishnan and N. Mathur, Phys. Rev. Lett. **132**, 20 (2024).
- [22] A. Radhakrishnan, M. Padmanath and N. Mathur, Phys. Rev. D. **110**, (2024).
- [23] W.Y. Liu, H.X. Chen and E. Wang, Phys. Rev. D. **107**, 054041 (2023).
- [24] F.L. Wang, R. Chen and X. Liu, Phys. Lett. B. **835**, 137502 (2022).
- [25] X. Chen and L. Ma, arXiv:2410.13775 [hep-ph].
- [26] F.K. Guo, C. Hanhart, U.G. Meißner, Q. Wang, Q. Zhao and B.S. Zou, Rev. Mod. Phys. **90**, 015004 (2018), [erratum: Rev. Mod. Phys. **94**, 029901 (2022)].
- [27] X.K. Dong, F.K. Guo and B.S. Zou, Commun. Theor. Phys. **73**, 125201 (2021).
- [28] X.K. Dong, F.K. Guo and B.S. Zou, Progr. Phys. **41**, 65 (2021).
- [29] H.X. Chen, W. Chen, X. Liu, Y.R. Liu and S.L. Zhu, Rept. Prog. Phys. **86**, 026201 (2023).
- [30] A. Manohar and H. Georgi, Nucl. Phys. B. **234**, 189 (1984).
- [31] J. Vijande, F. Fernandez and A. Valcarce, J. Phys. G. **31**, 481 (2005).
- [32] F. Wang, G.h. Wu, L.j. Teng and J.T. Goldman, Phys. Rev. Lett. **69**, 2901 (1992).
- [33] F. Wang, J.l. Ping, G.h. Wu, L.j. Teng and J.T. Goldman, Phys. Rev. C. **51**, 3411 (1995).
- [34] E. Hiyama, Y. Kino and M. Kamimura, Prog. Part. Nucl. Phys. **51**, 223 (2003).
- [35] E. Hiyama and M. Kamimura, Front. Phys. (Beijing) **13**, 132106 (2018).
- [36] C.R. Deng, J.L. Ping and F. Wang, Phys. Rev. D. **90**, 054009 (2014).
- [37] M. Cleven, F.K. Guo, C. Hanhart, Q. Wang and Q. Zhao, Phys. Rev. D **92**, 014005 (2015).
- [38] C.R. Deng, H. Chen and J.L. Ping, Phys. Rev. D. **101**, 054039 (2020).
- [39] C.R. Deng, Phys. Rev. D. **105**, 116021 (2022).
- [40] J. Wei, Y.H. Wang, C.S. An and C.R. Deng, Phys. Rev. D. **106**, 096023 (2022).
- [41] Y.H. Wang, J. Wei, C.S. An and C.R. Deng, Chin. Phys. Lett. **40**, 021201 (2023).
- [42] Z.H. Lin, C.S. An and C.R. Deng, Phys. Rev. D. **109**, 056005 (2024).
- [43] C.R. Deng and C.S. An, Phys. Rev. D. **111**, 034002 (2025).
- [44] M.L. Du, W. Chen, X.L. Chen and S.L. Zhu, Phys. Rev. D. **87**, 014003 (2013).
- [45] H.X. Chen, Commun. Theor. Phys. **74**, 125201 (2022).
- [46] H.X. Chen, arXiv:2501.16603 [hep-ph].